Journal of Alloys and Compounds, 207/208 (1994) 165–169
JALCOM 3031

Rare earth energy levels and magnetic properties of $DyPO_4$

C.-K. Loong, L. Soderholm and J. Simon Xue
Argonne National Laboratory, Argonne, IL 60439 (USA)

M.M. Abraham and L.A. Boatner
Oak Ridge National Laboratory, Oak Ridge, TN 37831 (USA)

Abstract

The dynamic and static paramagnetic response of $DyPO_4$ has been studied by neutron inelastic scattering and single-crystal magnetic susceptibility measurements. The observed energies and intensities of the magnetic transitions at 15 and 100 K were used to refine the parameters of the crystal field potential for Dy^{3+} ions in $DyPO_4$. The derived crystal field level structure provides a basis for explaining the low temperature magnetic properties of this compound.

1. Introduction

$DyPO_4$ crystallizes in the tetragonal zircon structure (space group $I4_1/amd$) in which four equivalent rare earth ions in a unit cell occupy sites of D_{2d} point-group symmetry. Similar to the isostructural compounds $TbPO_4$ and $HoPO_4$, $DyPO_4$ exhibits a number of intriguing magnetic properties at low temperatures. In the absence of an applied magnetic field, $DyPO_4$ orders antiferromagnetically with the Dy moments oriented parallel and antiparallel to the crystallographic c-axis at temperatures $T < T_N = 3.4$ K [1–5]. Below T_N, an antiferromagnetic (af) to paramagnetic (pm) phase transition can be induced by a magnetic field applied along the c-axis for which the af-pm phase boundary joining (T_N, 0) and the tricritical point ($T_T \approx 2$ K, $H_T \approx 0.7$ T) in the H–T phase diagram has been established [4–10]. The nature of the spin structure and phase transitions in the region of mixed metamagnetic phases, ($T < T_T$, $0.5 < H < 1$ T), however, is not yet understood.

The crystal field (CF) states and the spin dynamics of the Dy^{3+} ions have important consequences for the magnetic and luminescence properties of $DyPO_4$. In spite of numerous prior studies employing various experimental methods, information regarding the CF-split ground-multiplet wavefunctions of the Dy^{3+} ions in $DyPO_4$ is still incomplete. From neutron diffraction [1–5], optical absorption [11–14] and Mössbauer effect [15] studies, the ground state is known to have large $|15/2, \pm 15/2\rangle$ components and spectroscopic splitting g-factors parallel and perpendicular to the c-axis given by $g_\parallel = 19$ and $g_\perp = 0$, respectively. The saturated magnetic moment of the ground state doublet was estimated to be 9.2 μ_B at 0 K [1,3]. The energies and symmetries of all other states are not known. The first excited state was estimated to be about 8 meV above the ground state [14]. Consequently, the magnetic behavior has been interpreted by Ising-like interactions of magnetic ions with effective spins of 1/2. Since the excited states are ignored in this approach, only the very low-temperature data can be analyzed quantitatively [16–21]. Recently, we have initiated a systematic study of the rare earth energy-level structure of the RPO_4 (R = Tb to Yb) compounds. In the present paper, we report inelastic neutron scattering and magnetic susceptibility measurements along with a corresponding determination of the crystal field parameters.

2. Experimental details

Approximately 80 g each of polycrystalline powders of $DyPO_4$ and $LuPO_4$ were prepared by the technique of precipitation from molten urea [22]. The powders were then pressed into pellets and annealed at 1200 °C in air for 24 h to improve the crystalline quality. The samples were examined by X-ray powder diffraction and were found to have the appropriate zircon structure [23]. No impurity phases were observed within the experimental uncertainty. Single crystals were grown by dissolving and reacting the appropriate rare earth oxide in molten lead pyrophosphate at high temperatures [24]. The magnetic susceptibility of a 0.93 mg single crystal was measured with an applied field of

0925-8388/94/$07.00
SSDI 0925-8388(94)03031-D

500 G oriented perpendicular and parallel to the crystallographic c-axis using a SQUID magnetometer.

Inelastic neutron scattering measurements were performed using the HRMECS chopper spectrometer at the Argonne spallation neutron source IPNS. The experimental procedures were the same as those described previously in the crystal field (CF) study of RPO_4 compounds [25]. The energy resolution, ΔE (full-width-at-half-maximum), of the HRMECS spectrometer varies with energy transfer but is approximately 2–4% of the incident neutron energy (E_0) over the neutron energy-loss spectrum. To fully explore the CF and phonon excitations up to 150 meV, five incident energies, 3.8, 20, 40, 60, and 200 meV were chosen for the studies at selected temperatures between 4.2 and 100 K. The magnetic origin of the CF peaks was identified by an examination of the temperature and momentum-transfer dependence of the observed intensities and by a comparison with the spectra of the non-magnetic, isostructural compound $LuPO_4$. The data were corrected for background scattering and the effect of sample self-shielding by subtracting the combined empty-container and neutron absorber (*i.e.* cadmium) runs. Measurements of the elastic incoherent scattering from a vanadium standard provided detector calibration and intensity normalization.

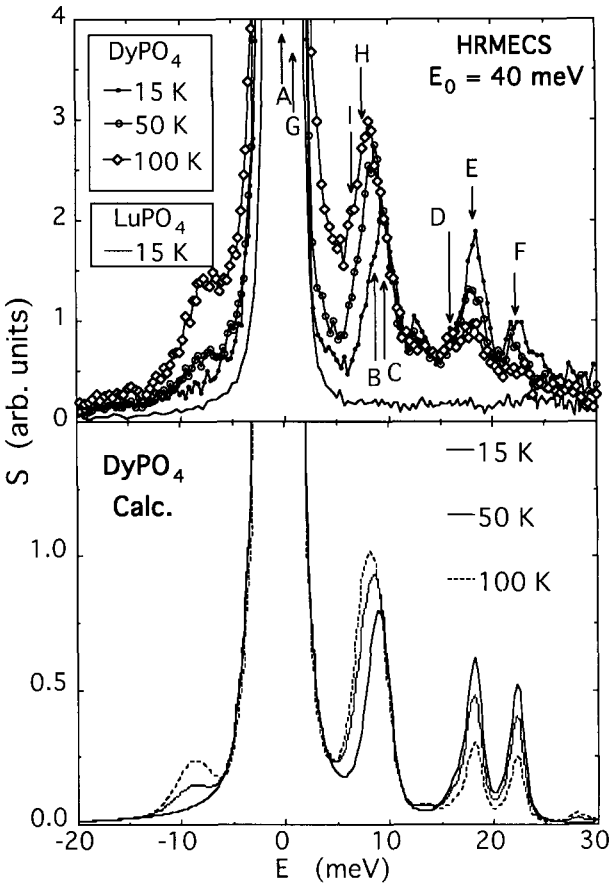

Fig. 1. Upper panel: the measured scattering functions for $DyPO_4$ and $LuPO_4$. The datapoint errors are approximately the size of the symbols. The lines for the $DyPO_4$ data are guides to the eye. The labeled peaks correspond to the CF transitions shown in Fig. 2. Lower panel: the corresponding calculated scattering functions for CF transitions.

3. Results and discussion

The $Dy^{3+}{}^6H_{15/2}$ ground multiplet of $DyPO_4$ is split by the tetragonal CF into four Γ_6 and four Γ_7 Kramers doublets. Excitations (or de-excitations) between any two doublet states and elastic scattering within a doublet are allowed by the selection rules for magnetic dipole transitions in a neutron scattering experiment. Transitions to the next multiplet, $^6H_{13/2}$, which is located at energies over 430 meV, were not observable in the present neutron experiment. The observed (magnetic and phonon) spectra for $DyPO_4$ obtained at 15, 50, and 100 K with an incident energy of 40 meV are shown in the upper panel of Fig. 1. The spectrum of non-magnetic $LuPO_4$, also shown in Fig. 1, provides an estimate of the underlying phonon component in $DyPO_4$. Strong peaks at 0, 9.5, 18.2 and 22.3 meV and weak features at about 12.4 and 16 meV were observed at 15 K. There is also evidence of a strong, unresolved peak at about 8.5 meV, as indicated by the asymmetric peak profile. The fact that the intensities of these peaks decrease at higher temperatures (*e.g.* 50 and 100 K) indicates that they originate from CF excitations of the ground state. The additional intensities in the 5–7.5 meV region which only occurred at higher temperatures, on the other hand, result from transitions from low-lying excited states. No sharp CF excitations of discernible intensity at energies below 8 meV or above 30 meV were found from the runs with E_0 of 3.8, 20, 60 and 200 meV.

The observed position of a CF peak is equal to the energy separation of the two CF states (*e.g.* $\langle i|$ and $\langle j|$) that participate in the transition, and the intensity is proportional to the square of the matrix element $\langle i|J_\perp|j\rangle$ (where $J_\perp$ is the component of the total angular momentum operator perpendicular to the neutron wavevector). If the CF-state energies and wavefunctions are obtained from a diagonalization of a Hamiltonian which contains a parameter set for the CF potential, the neutron scattering function, $S(E)$, can be calculated in a straightforward manner. Details concerning the neutron scattering cross-section, the relation between the observed transition strength, and the spectroscopic splitting g-factors have been given elsewhere [25]. In practice, the CF parameters for the system under study are not known, and the goal is to find a set of CF parameters that produces calculated spectra which are

consistent with the observed CF peak energies and intensities at all temperatures.

The CF model employed here represents a single rare earth ion in a crystalline environment. The formulation is based on the scheme of intermediate coupling using spherical tensor techniques. The Hamiltonian, associated parameters, and underlying assumptions of the theory have been treated in detail elsewhere [26–27]. The diagonalization of the total Hamiltonian was executed by a computer code written by the Crosswhites [27]. The 99 lowest free-ion Russell–Saunders states were used to calculate the required matrix elements. The parameters for the free-ion part of the Hamiltonian were taken from those obtained previously for Dy-doped LaF_3 from optical spectroscopy by Carnall *et al.* [28] and were fixed throughout the calculations.

The Dy ion site-symmetry (D_{2d}) in $DyPO_4$ necessitates the use of five parameters, B_0^2, B_0^4, B_4^4, B_0^6 and B_4^6 to characterize the CF part of the Hamiltonian. In order to fit the neutron spectra, a set of CF parameters was obtained for $DyPO_4$ by scaling the parameters established previously for $TbPO_4$ [29]. Scaling of the CF parameters between different isostructural rare earth compounds has been described [30] previously in the CF treatments of high T_c superconductors. A comparison of the observed data with the calculated spectra at 15, 50, and 100 K using the parameters ($B_0^2 = 342$, $B_0^4 = 109$, $B_4^4 = -695$, $B_0^6 = -733$ and $B_4^6 = -105$ cm^{-1}) obtained from this scaling favored the assignment of 8.5, 9.5, 16.0, and 18.2 meV as the energies of the first four excited states above the ground state. A subsequent fit to the neutron data converged rapidly, yielding calculated energies and intensities in good agreement with the experimental results for all of the transitions with the exception of the weak feature at 12.4 meV which was not accounted for by the calculations. The crystal field parameters corresponding to the best fits, $B_0^2 = 308.2$, $B_0^4 = 102.2$, $B_4^4 = -716.3$, $B_0^6 = -735.7$ and $B_4^6 = -25.5$ cm^{-1}, are comparable to those found for the isostructural compounds $TbPO_4$ and $HoPO_4$ [25,29]. The calculated magnetic neutron scattering spectra are displayed in the lower panel of Fig. 1, and the resulting crystal field level scheme for the $Dy^{3+}{}^6H_{15/2}$ ground multiplet is shown schematically in Fig. 2. An assumed intrinsic width of 0.75 meV for the CF peaks was used. Details concerning the magnetic form factor and the instrumental resolution functions in use have been described previously, and the procedures have been thoroughly tested for the Tb, Ho, Er, and Tm phosphates [25,29,31]. Since dysprosium has a large neutron absorption cross-section (940 barns at neutron energy of 70 meV), an effective attenuation factor of $\exp(-5.578/\sqrt{E_f})$ was applied to calculate the scattered intensity as a function of energy transfer (E_f is the neutron final energy in meV). Such a factor was used in order to

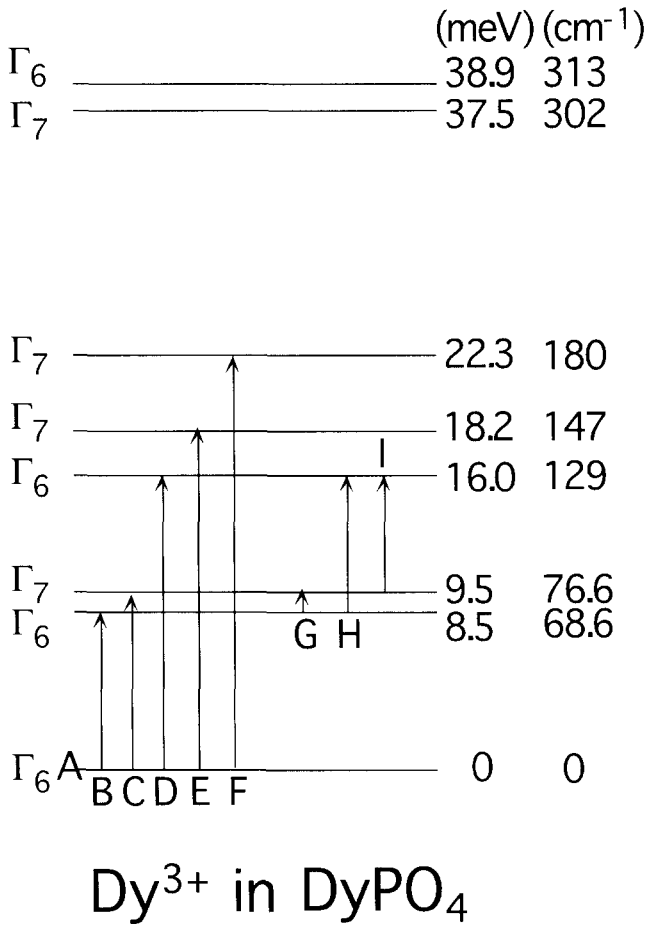

Fig. 2. A schematic diagram of the splitting of the $Dy^{3+}{}^6H_{15/2}$ ground multiplet by the crystal field into four Γ_6 plus four Γ_7 Kramers doublets. The transition labels refer to the experimentally observed transitions shown in Fig. 1.

reproduce the 41% effective transmission of the neutron beam that was determined in the 40 meV runs.

In general, the agreement between the observed and calculated spectra at all three temperatures, as shown in Fig. 1, is good. The calculated matrix elements connecting the ground state to the upper Γ_7 and Γ_6 states near 38 meV (see Fig. 2) are exceedingly small. This explains the lack of observed magnetic intensity above 30 meV in the neutron spectra. On the other hand, excitation from the Γ_7 state at 9.5 meV to the Γ_7 at 37.5 meV results in a weak feature at 28 meV at high temperatures (Fig. 1). This very weak feature is difficult to resolve experimentally because the phonon background also increases at high temperatures. The weak peak at 12.4 meV and the excess intensities below 5 meV at 50 and 100 K in the observed spectra, however, were not accounted for by the CF calculations. In an attempt to assess the extent to which these features can be accommodated by the CF model, we have extensively searched over the parameter space with a fit that included a 12.4 meV excitation, a fit that replaced the 16 meV line by a 12.4 meV line, and a fit that

included additional low-lying levels below 5 meV. In no case could we find a calculated spectrum that remotely resembled the observed energies and intensities. Therefore, we are confident that the overall magnetic excitation spectra are best represented by the CF model using the CF parameters mentioned above. The extra features may arise from coupling of CF states to other elementary excitations (*e.g.* phonons), which is not considered by the single-ion CF model. The present experiment using polycrystalline samples does not provide sufficient sensitivity for a quantitative evaluation of these effects.

In Fig. 3, the magnetic susceptibility determined from a single crystal of $DyPO_4$ is compared with the calculated susceptibility obtained from the van Vleck formalism [32] using the final CF parameters. The good agreement between the observed and calculated susceptibility lends credence to the correctness of the CF interpretation of the neutron data. The deviation of the observed $\chi_{\parallel}$ from the calculated values at $T < 50$ K, which is also seen [25,29] in $TbPO_4$ and $HoPO_4$, is caused by the internal field of the exchange interactions which eventually leads to the antiferromagnetic ordering at 3.4 K. The large anisotropy, $\chi_{\parallel}$ versus $\chi_{\perp}$ or $g_{\parallel}$ ($= 19.4$) versus $g_{\perp}$ (≈ 0), is a consequence of the 99% pure $|15/2, \pm 15/2\rangle$ components in the Γ_6 ground state doublet. The calculated saturated moment (at 0 K) is 9.7 μ_B This magnetic ground state, well separated from the higher states (see Fig. 2), justifies the analyses of the low temperature magnetic properties of $DyPO_4$ using the corresponding g-factors with an effective spin of $\pm 1/2$ in the molecular field and Ising approximations [16–21].

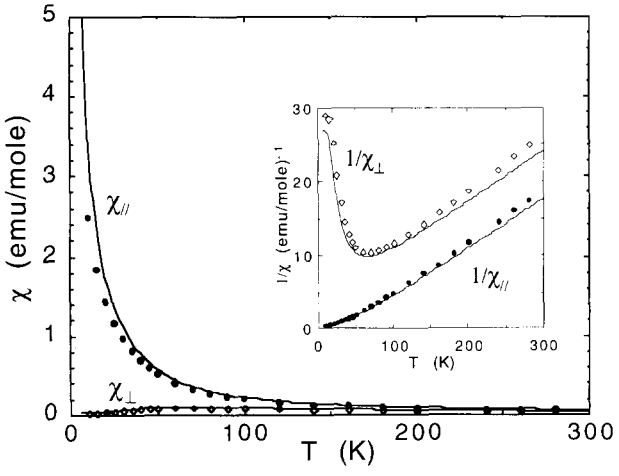

Fig. 3. The calculated (solid curves) and measured (symbols) magnetic susceptibility of $DyPO_4$ with the applied magnetic field oriented perpendicular and parallel to the crystallographic c-axis. Inset: The inverse magnetic susceptibility.

Acknowledgment

Work performed at Argonne and Oak Ridge National Laboratories is supported by the U.S. DOE, Basic Energy Sciences under Contract Nos. W-31-109-ENG-38 and DE-AC05-840R21400, respectively.

References

1 H. Fuess, A. Kallel and F. Tchéou, *Solid State Commun., 9* (1971) 1949.
2 G. Will, W. Schäfer, W. Scharenberg and H. Göbel, *Z. Angew. Phys., 32* (1971) 122.
3 W. Scharenberg and G. Will, *Int. J. Magnetism, 1* (1971) 277.
4 N. Schibuya, K. Knorr, H. Dachs, M. Steiner and B.M. Wanklyn, *Solid State Commun., 17* (1975) 1305.
5 A.H. Millhouse, M. Steiner and H. Dachs, *J. Appl. Phys., 50* (1979) 2011.
6 P.J. Becker, I.R. Jahn and S.H. Smith, *J. Phys. C, 9* (1976) L505.
7 J.E. Battison, A. Kasten, M.J.M. Leask and J.B. Lowry, *Solid State Commun., 17* (1975) 1363.
8 I.R. Jahn, J. Ferré, M. Régis and Y. Farge, *Solid State Commun., 28* (1978) 421.
9 J. Hoffmann, *Phys. Status Solidi B, 165* (1991) 517.
10 M. Regis, J. Ferre, Y. Farge and I.R. Jahn, *Physica B, 86–88* (1977) 599.
11 J.C. Wright and H.W. Moss, *J. Appl. Phys., 41* (1970) 1244; *Phys. Lett., 29A* (1969) 495.
12 G.A. Prinz, J.F.L. Lewis and R.J. Wagner, *Phys. Rev. B, 10* (1974) 2907; G.A. Prinz and R.J. Wagner, *J. Appl. Phys., 42* (1971) 1569.
13 C.J. Ellis, M.J.M. Leask, D.M. Martin and M.R. Wells, *J. Phys. C, 4* (1971) 2937.
14 I.R. Jahn and S.H. Smith, *Phys. Status Solidi B, 68* (1975) 531.
15 D.W. Forester and W.A. Ferrando, *Phys. Rev. B, 13* (1976) 3991.
16 J.H. Colwell, B.W. Mangum, D.D. Thornton, J.C. Wright and H.W. Moss, *Phys. Rev. Lett., 23* (1969) 1245.
17 G.T. Rado, *Solid State Commun., 8* (1970) 1349.
18 J.C. Wright, H.W. Moos, J.H. Colwell, B.W. Mangum and D.D. Thornton, *Phys. Rev. B, 3* (1971) 843.
19 C.S. Koonce, B.W. Mangum and D.D. Thornton, *Phys. Rev. B, 4* (1971) 4054.
20 M.J. Metcalfe and H.M. Rosenberg, *J. Phys. C, 5* (1972) 450.
21 M. Schienle, A. Kasten and P.H. Müller, *Phys. Status Solidi, 119* (1983) 611.
22 M.M. Abraham, L.A. Boatner, T.C. Quinby, D.K. Thomas and M. Rappaz, *Radioactive Waste Management, 1* (1980) 181.
23 W.O. Milligan, D.F. Mullica, G.W. Beall and L.A. Boatner, *Inorg. Chim. Acta, 70* (1983) 133.
24 R.S. Feigelson, *J. Am. Ceram. Soc., 47* (1964) 257.
25 C.-K. Loong, L. Soderholm, J.P. Hammonds, M.M. Abraham, L.A. Boatner and N.M. Edelstein, *J. Phys.: Condensed Matter, 5* (1993) 5121.
26 B.G. Wybourne, *Spectroscopic Properties of Rare Earths*, Wiley, New York, 1965.
27 H.M. Crosswhite and H. Crosswhite, *J. Opt. Soc. Am., B1* (1984) 246.

28 W.T. Carnall, G.L. Goodman, K. Rajnak and R.S. Rana, *J. Chem. Phys., 90* (1989) 3443.
29 C.-K. Loong, L. Soderholm, G.L. Goodman, M.M. Abraham and L.A. Boatner, *Phys. Rev. B, 48* (1993) 6124.
30 L. Soderholm, C.-K. Loong, G.L. Goodman and B.D. Dabrowski, *Phys. Rev. B, 43* (1991) 7923; G.L. Goodman, C.-K. Loong and L. Soderholm, *J. Phys.: Condensed Matter, 3* (1991) 49.
31 C.-K. Loong, L. Soderholm, M.M. Abraham, L.A. Boatner and N.M. Edelstein, *J. Chem. Phys., 98* (1993) 4214.
32 J.H. van Vleck, *The Theory of Electric and Magnetic Susceptibilities*, Oxford University Press, London, 1932.